PCCP

ROYAL SOCIETY OF CHEMISTRY

PAPER

View Article Online
View Journal | View Issue

Check for updates

Cite this: *Phys. Chem. Chem. Phys.*, 2024, **26**, 25208

Adsorption of rare bases on transition metal doped γ-graphyne nanosheets: a DFT study†

Xia Zeng,[a] Ruiying Zhang,[a] Ruirui Li,[a] Ruimei Li,*[b] Hong Cui,[c] Caibin Zhao,[a] Shengrui Zhang[a] and Lingxia Jin*[a]

Received 7th August 2024,
Accepted 13th September 2024

DOI: 10.1039/d4cp03128h

rsc.li/pccp

Detection of rare bases (RBs) is key to understanding biological complexity, rapidly diagnosing genetic diseases and advancing personalized medicine. Electrochemical sensors are one of the most promising methods for RB detection, but their low responsiveness limits their effectiveness. Therefore, enhancing selectivity and sensitivity is necessary. γ-Graphyne (γ-GY) has garnered significant attention due to its sp^2 and sp hybrid carbon bonds and layered two-dimensional planar structure, as well as its extensive conjugated system, and sizable triangular hole. In this study, the structural characteristics, electronic properties, and sensing parameters of the adsorption involving RBs with both γ-GY and transition metal (Fe, Co, and Ni)-doped γ-graphyne (TM-GY) nanosheets are investigated using density functional theory calculations to evaluate the potential of nanosheets for sequencing RBs in DNA. The result shows that the adsorption interaction between RBs and γ-GY is weak physical adsorption, making it difficult to distinguish RBs. In contrast, the adsorption of RBs with TM-GY is stronger chemisorption and can be completely separated by translocation time and sensing response. Through translocation time calculations, we demonstrate the high selectivity of Ni-GY for RBs. Furthermore, sensitivity analysis reveals that Fe-GY exhibits excellent responsiveness to RBs. Our work reveals that the TM-GY nanosheets hold promise for detecting RBs compared with the γ-GY, and may provide valuable insights for the design of graphyne-based biosensors and catalysts.

Published on 24 September 2024. Downloaded on 4/12/2026 3:20:09 PM.

1. Introduction

Understanding the interactions of biomolecules with carbon-based materials is essential for developing various chemical sensing and molecular recognition materials for applications. Apart from the four basic bases, there are some less abundant bases in DNA called rare bases (RBs), and many RBs are methylated bases, which are chemical modifications of common bases.[1] The methylated bases are important epigenetic DNA markers and play a key role in gene expression.[2] For instance, they can regulate silenced gene expression, modulate chromatin compaction, influence protein–DNA interactions, and impact DNA repair and stability, among other functions.[3,4] The most significant DNA methylation alteration that takes place at the cytosine C5 location is 5-methylcytosine (5-meCyt), also referred to as the "fifth base".[5] The demethylation process of 5-meCyt involves intermediates such as 5-hydroxymethylcytosine (5-hmCyt), 5-carboxycytosine (5-caCyt), and 5-formylcytosine (5-fCyt). DNA methylation and demethylation processes exist in a state of dynamic equilibrium. Normal DNA methylation participates in various cellular processes, while aberrant methylation can lead to abnormalities in gene expression, which could result in a range of malignant illnesses.[6–9] Early and accurate diagnosis is essential for guiding the treatment and improving the cure rate of major genetic diseases and cancers. However, the RBs not only have very low content but also have high structural similarity. Moreover, existing methods have disadvantages such as being time-consuming, having low sensor response, and poor detection specificity, which limit their wide clinical application.[10,11] Therefore, developing a sensing material with high selectivity and reactivity for recognizing RBs is valuable theoretical and practical work.

With the emergence of graphene,[12] numerous novel two-dimensional (2D) materials have been developed, including fullerene,[13] silicene,[14] h-BN,[15] MoS_2,[16] phosphorene,[17] and so on, which are widely used in the electronics, photovoltaics, and medical industries, and in the construction of sensors due to the advantages of specific surface area, excellent electrical conductivity and superior electron trapping ability.[18–21] Furthermore, most 2D materials can significantly improve the

[a] *Shaanxi Key Laboratory of Catalysis, School of Chemical & Environment Science, Shaanxi University of Technology, Hanzhong 723001, China. E-mail: Rae@snut.edu.cn, jinlx@snut.edu.cn; Tel: +86-916-2641660*
[b] *School of Mathematics & Computer Science, Hanzhong 723001, China*
[c] *School of Mechanical Engineering, Shaanxi University of Technology, Hanzhong 723001, China*

† Electronic supplementary information (ESI) available. See DOI: https://doi.org/10.1039/d4cp03128h

This journal is © the Owner Societies 2024

Published on 24 September 2024. Downloaded on 4/12/2026 3:20:09 PM.

detection capabilities of the sensing devices used to detect metal ions,[22] gases,[23,24] and biomolecules.[25] Nevertheless, these materials have certain flaws of their own. The strong dependence on the environment of phosphene severely limits its applications in sensors and other electronic devices. Graphene, consisting of sp^2-hybridized carbon atoms, possesses outstanding electronic conductivity attributed to its delocalized π-electrons. However, as a semimetal with a zero-band gap, its application in susceptible electrical detection of biomolecules is constrained. Fortunately, graphyne (GY) and its family are theoretically predicted to be semiconductor materials with the potential to rival graphene in the realm of electronic applications. Although both are carbon materials, they have different structural and electronic properties due to the different arrangement of carbon atoms. Depending on the alkyne bond inserted, different GY structures can be obtained, such as α-, β-, γ-, δ-GY, *etc.* Compared with graphene, γ-GY has a large triangular ring of 18 carbons with an extensive π-conjugation system, which is constituted by the fusion of benzene rings and alkyne linkages. This distinct arrangement endows γ-GY with a pronounced adsorption capacity for biomolecules. As an intrinsic semiconductor carbon material with a band gap and better structural stability, γ-GY is more suitable for fabricating electronic nanodevices than other kinds of GY.

Back in 1987, Baughman proposed graphyne and its derivative, a novel type of carbon substance formed by a combination of C_{sp} and C_{sp^2} atoms.[26] In 2010, Li *et al.* prepared a smooth, uniform, and continuous 2D carbon material graphdiyne (GDY) by a wet chemical method.[27] In 2016, the GY and its derivatives were initially used in the areas of bio-sensing, bio-imaging, cancer therapy, and radiation protection.[28] Later, Li *et al.* synthesized γ-GY by mechanochemistry, which greatly promoted its development.[29] GY and its derivatives have been extensively studied in the detection of biological molecules, especially the detection of bases.[30,31] For instance, S. Madhumitha *et al.*[32] researched the binding of cytosine and guanine on pure and boron-substituted γ-GY nanosheets, showing that both types of nanosheets exhibit effective adsorption towards these nucleobases. Furthermore, Rameshwar *et al.*[33] explored the potential application of atomically thin GDY as a DNA sequencing platform for nanopore technology. This study demonstrated that the GDY-based nanopore (GDYNP) system can accurately detect nuclear bases by measuring their particular translocation time within the GDYNP device. Then, Shekar *et al.*[34] studied the interaction of individual nucleobases and nucleobase pairs with both GY and GDY by DFT. It was found that the relative interaction strength of the nucleobases with GY and GDY followed the order G > A > C > T > U, and for base pairs, GC > AT > AU. Previously, our research mainly focused on the adsorption behavior of pristine and boron/nitrogen-substituted γ-GY with RBs and RB pairs. The results indicate that boron/nitrogen-doped γ-GY has the potential to distinguish rare bases to a certain extent.[35,36]

Although numerous 2D materials have been investigated as substrates for bases or base pairs, previously published reports[32–36] have not addressed the adsorption of RBs with the transition metal doped γ-graphyne (TM-GY) nanosheets. It is well known that doping represents a highly effective strategy for enhancing the properties of materials. Among the TM atoms, Fe, Co, and Ni stand out for their relatively small atomic size. They can not only be stably adsorbed in γ-GY, but also have great potential to significantly improve the chemical reactivity and conductivity of the surface by adjusting the electronic structure.[20,24] In addition, these elements are abundant and cost-effective, offering an ideal choice for economical and efficient material modification. It is conceivable that if graphyne is doped with Fe, Co, and Ni atoms, it could become a potential 2D material for the detection of RBs. In this study, we explore the interactions of RBs adsorbed on γ-GY and TM-GY systems using density functional theory (DFT). First, the active site of TM-GY is identified, followed by an assessment of its chemical stability through cohesive energy (E_{coh}) calculations. The most stable conformation of the RBs on TM-GY is then determined using the adsorption energy (E_{ads}). The electronic structural properties of the system are analyzed through charge transfer (Q), band structure, partial density of states (PDOS), and charge differential density (CDD) evaluations. Additionally, from an experimental perspective, we assess the system's translocation time (τ) and sensitivity response (S%). The results indicate that these TM-GY materials possess excellent electronic properties, which can effectively assist in distinguishing each target RB molecule. This may help us successfully distinguish various biomolecules and provide important theoretical guidance for the creation of biomolecular devices founded on carbon-based materials.

2. Computational details

In this work, DMol^3 software is used to carry out structure optimization and electronic analyses employing density functional theory (DFT).[37] The GGA-PBE exchange–correlation functional method is performed for the adsorption calculation of RBs with the γ-GY and TM-GY nanosheets.[38,39] The Grimme dispersion correction is used to deal with the long-range van der Waals interactions on γ-GY and TM-GY surfaces.[40,41] The polarized double numerical (DNP) atomic basis set and spin unrestricted approximation are selected to solve the self-consistent field. The correction for Basis Set Superposition Error (BSSE) was not included in the current work because the value of BSSE is very small in the DNP basis set.[42] All systems are fully relaxed and optimized until the total energy convergence threshold of 2×10^{-5} Ha, the maximum force criterion of 0.004 Ha Å^{-1}, and the maximum displacement criterion of 0.005 Å. The 20 Å vacuum separation is used to avoid interactions between adjacent layers along the *c*-axis. In the study, a 450 eV cut-off and $10 \times 10 \times 1$ k points are taken into account for Brillouin zone sampling in electronic structure calculations.[43]

Cohesive energy (E_{coh})[44] is utilized to evaluate the stability of both γ-GY and TM-GY nanosheets, as described in eqn (1):

$$E_{coh} = \frac{(E_T - xE_C - yE_{TM})}{n} \quad (1)$$

Published on 24 September 2024. Downloaded on 4/12/2026 3:20:09 PM.

where E_T, E_C, and E_{TM} are the overall energy of the system, the total energy of several C atoms, and the energy of the doped TM atoms, respectively. The terms "n," "x," and "y" represent the total number of atoms in the system, the number of C atoms in the system, and the doped number of transition metal atoms, respectively.

The adsorption can be carried out in two different ways: the active center is perpendicular to the substrate, and the active center is parallel to the substrate, respectively. The adsorption energy (E_{ads})[45] can be defined as eqn (2):

$$E_{ads} = E_{\gamma\text{-GY–RB}} - E_{\gamma\text{-GY}} - E_{RB} \quad (2)$$

where $E_{\gamma\text{-GY–RB}}$, $E_{\gamma\text{-GY}}$, and E_{RB} refer to the overall energy of the rare base molecule on the γ-GY nanosheets, γ-GY, and rare base molecule, respectively.

The translocation time (τ)[46] refers to the duration from the beginning of the process to produce a steady signal, which is closely associated with the adsorption energy. The translocation time is determined by eqn (3)

$$\tau = {\nu_0}^{-1} \exp\left(\frac{-E_{ads}}{k_B T}\right) \quad (3)$$

where ν_0, T, and k_B refer to the operation frequency (10^{16} s^{-1}), the temperature (300 K), and the Boltzmann constant (8.62×10^{-5} eV), respectively.[47]

Another crucial factor is the sensing response, which is directly linked to electrical conductivity (σ).[48] The calculation is determined by eqn (4):

$$\sigma \propto \exp\left(-\frac{E_g}{2k_B T}\right) \quad (4)$$

where σ, E_g, and $k_B T$ are the conductivity, the energy gap, and the thermal energy, respectively.

The sensing response ($S\%$)[49] varies in accordance with the alteration in conductivity. The calculation is obtained by eqn (5):

$$S\% = \left|\frac{\sigma - \sigma_0}{\sigma_0}\right| \times 100\% \quad (5)$$

where σ_0 and σ are the conductivity of the RBs with γ-GY and TM-GY nanosheets, respectively.

3. Results and discussion

Previous research[20] indicates that γ-GY has a high level of mobility as a semiconductor, making it a promising candidate for electrical sensor materials. Thus, the structural and electrical properties of γ-GY and TM-GY are analyzed, and the adsorption characteristics of RBs on these materials are subsequently revealed.

3.1 The structural and electronic properties of the γ-GY and TM-GY

The structures of the γ-GY and TM-GY are shown in Fig. 1. These structures are similar to graphene with hexagonal symmetry and are composed of two different types of sp^2 and sp hybrid carbon atoms. The γ-GY belongs to the D_{6h} point group

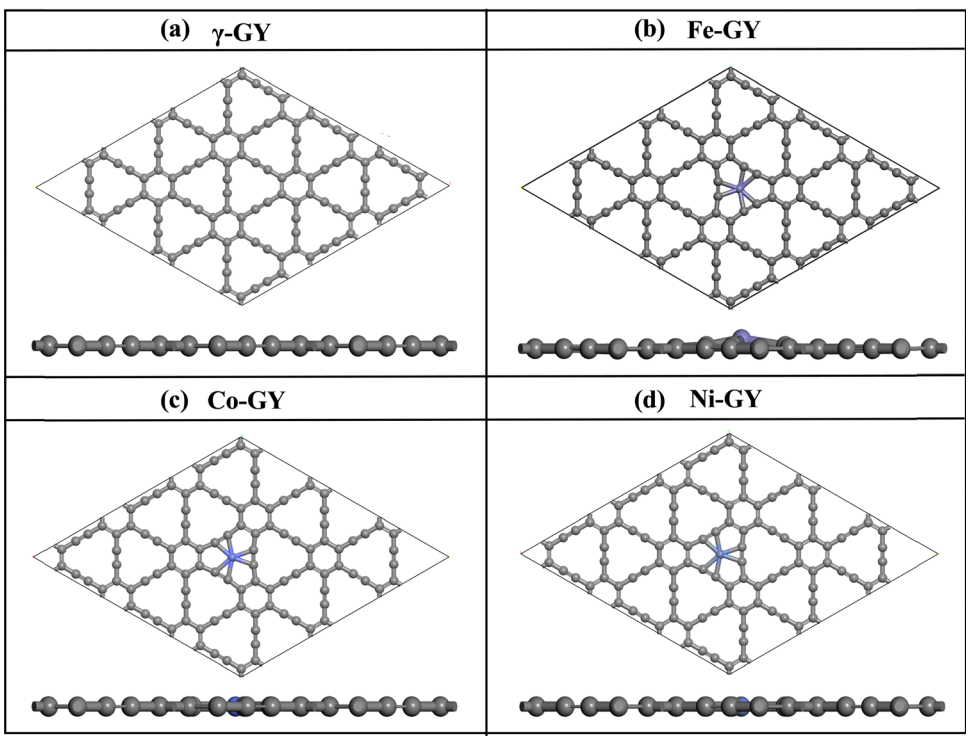

Fig. 1 Optimized geometries of the 3 × 3 × 1 supercell of (a) γ-GY, (b) Fe-GY, (c) Co-GY, and (d) Ni-GY nanosheets (top and side perspective).

 This journal is © the Owner Societies 2024

and the *P6/mmm* space group. The optimized lattice parameters for the primitive cell are determined as $a = b = 6.89$ Å. Within the hexagonal structure, the bond lengths for C_{sp^2}–C_{sp^2}, C_{sp^2}–C_{sp}, and C_{sp}–C_{sp} are measured to be 1.425, 1.408, and 1.225 Å,

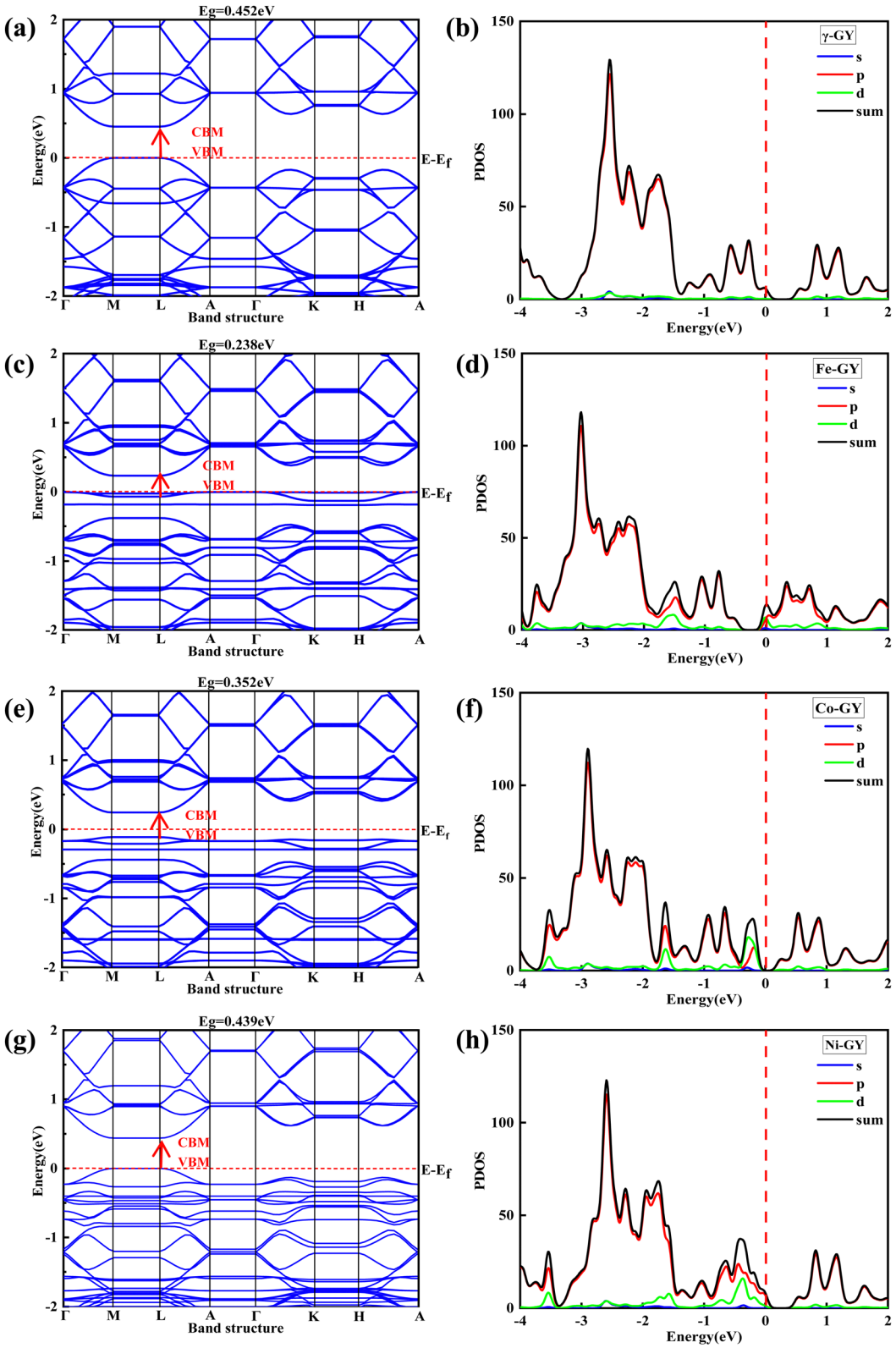

Fig. 2 Band structure (the left) of (a) γ-GY, (c) Fe-GY, (e) Co-GY, and (g) Ni-GY nanosheets, and DOS plot (the right) of (b) γ-GY, (d) Fe-GY, (f) Co-GY, and (h) Ni-GY nanosheets. The Fermi level is set to zero.

Published on 24 September 2024. Downloaded on 4/12/2026 3:20:09 PM.

Published on 24 September 2024. Downloaded on 4/12/2026 3:20:09 PM.

respectively. The band gap and PDOS of the γ-GY are shown in Fig. 2. This computational analysis confirms that the γ-GY is a semiconductor with an energy band gap of 0.452 eV, which aligns with earlier theoretical investigations.[32] The results show that γ-GY has a unique structure and excellent electrical properties, and is expected to have a broad application prospect in biosensing.

The cohesive energies of the γ-GY, Fe-, Co-, and Ni-doped γ-GY nanosheets are calculated to evaluate the stability of the doped system at values of −7.25, −7.22, −7.22, and −7.21 eV, respectively. Notably, the values are negative, proving that the γ-GY and TM-GY systems are stable. To find the optimal doping site for γ-GY systems, three different types of adsorption sites are considered (Fig. 3): hollow positions between H_1 and H_2, bridge positions between B_1, B_2, and B_3, and top positions between T_1 and T_2, respectively. According to previous studies,[50] the doping of transition metal atoms at the center of the alkyne ring of γ-GY is the most stable site, so our work only follows the doping of Fe, Co, and Ni atoms at the H_1 site. As shown in Fig. 1, when Fe, Co, and Ni are doped at the H_1 site of γ-GY, the adsorption energies are −3.48, −4.29, and −3.11 eV, respectively.

Remarkably, the 6 C_{sp} atoms exhibit a notable inclination towards the center TM atom within the TM-GY alkyne ring, resulting in the 6 TM–C_{sp} bonds of the same metal atom having comparable lengths. The bond lengths of Fe–C_{sp}, Co–C_{sp}, and Ni–C_{sp} are 1.97, 1.94, and 1.96 Å, respectively. According to the bond length statistics (Table 1), the TM–C_{sp} has the longest bond length, and there is no significant change between the C–C bond, suggesting that the TM atoms increase the specific surface area of γ-GY. This structural change may have some effects on γ-GY activity, such as providing more active sites and increasing electron mobility. Meanwhile, the X-ray diffraction (XRD) and scanning tunnel microscope (STM) images of the γ-GY and TM-GY are also shown in Fig. S1 and S2 (ESI†), which could complement other *ex situ* characterization methods to better match experimental images on this basis. These can not only provide a reference for experimental scientists to prepare and obtain high-quality GY but also provide an important research basis for the application of GY in the field of macroscopic devices.[51–53]

Table 1 The structural characteristics of γ-GY and TM-GY (bond lengths in Å, charges in *e*, and energy in eV)

System	C_{sp^2}–C_{sp^2}	C_{sp^2}–C_{sp}	C_{sp}–C_{sp}	TM–C_{sp}	E_{coh}	E_{ads}	Q	E_g
γ-GY	1.425	1.408	1.225	—	−7.25	—	—	0.452
Fe-GY	1.428	1.430	1.283	1.97	−7.22	−3.48	0.140	0.238
Co-GY	1.430	1.424	1.284	1.94	−7.22	−4.29	0.120	0.352
Ni-GY	1.426	1.423	1.273	1.96	−7.21	−3.11	0.130	0.439

Interestingly, when the TM atoms are adsorbed, the band gap of the TM-GY shifts upward, resulting in a smaller band gap than that of the γ-GY nanosheets (0.452 eV). The band gaps of the Fe-, Co-, and Ni-GY nanosheets are 0.238, 0.352, and 0.439 eV, respectively. As shown in Fig. 2, the band gap change of Fe-GY is the largest, followed by Co-GY, with Ni-GY being the smallest. The change in the gap is attributed to the interaction of the TM atoms and γ-GY, which in turn changes the electronic character and conductive ability of the system.

In the PDOS plot (Fig. 2), the valence electron orbitals of the C atoms and each TM atom are significantly widened and the highest peak value is also reduced under the doping of Fe, Co, and Ni atoms. Compared with γ-GY, the PDOS of TM-GY at the Fermi level shifts to the lower energy level, and the Fe-GY displacement is the largest. There is a significant DOS overlap between the TM atom and C atoms, suggesting the hybridization of TM atoms on the γ-GY nanosheets. Several new energy states are exhibited at the Fermi level of the C_{2p} orbital in the Fe-GY system (Fig. 4), which do not exist in the γ-GY, indicating the transfer of charge from Fe to the C_{2p} orbital. Subsequently, it is noted that the intensity of the energy states of the Fe_{4s} orbitals near the Fermi level decreases, which confirms the

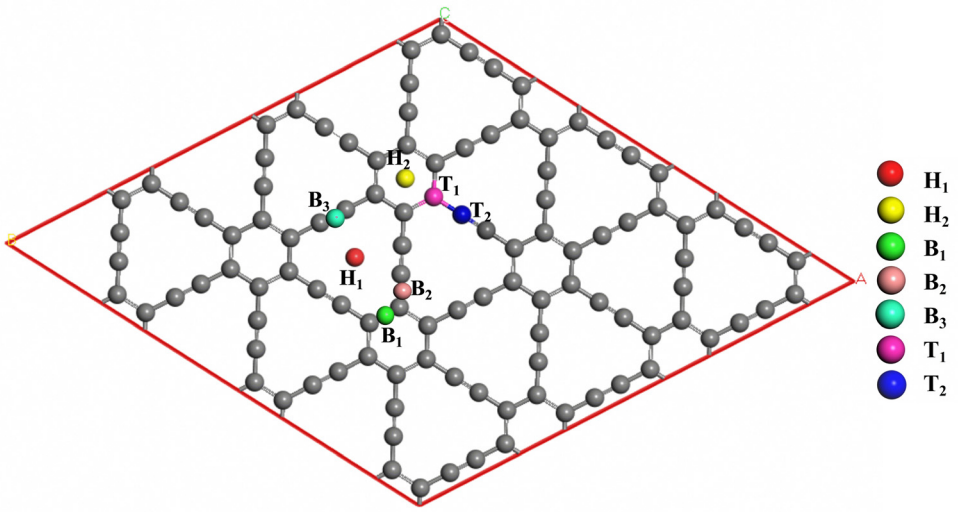

Fig. 3 Possible positions for the TM atom doped on γ-GY, where T_i, B_i, and H_i denote the top, bridge, and hollow sites, respectively.

 This journal is © the Owner Societies 2024

Published on 24 September 2024. Downloaded on 4/12/2026 3:20:09 PM.

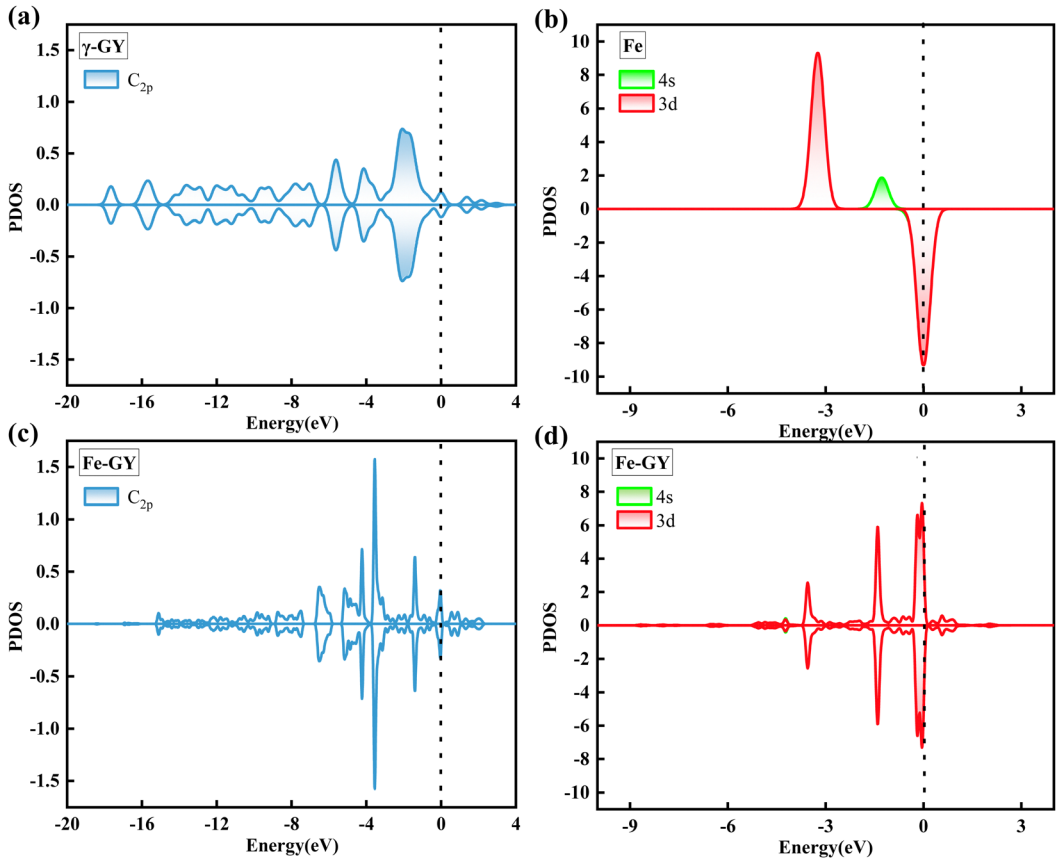

Fig. 4 PDOS plots: a comparison of the C_{2p} orbitals between (a) γ-GY and (c) Fe-GY in the left panel; a comparison of the Fe valence orbitals of (b) the standalone Fe atom with those within (d) the Fe-GY system in the right panel.

transfer of charge from the Fe valence orbital to the C_{2p} orbital in the Fe-GY system. Similar orbital interactions are observed for Co-GY and Ni-GY in Fig. S3 (ESI†). The change in PDOS near the Fermi level has a prominent impact on the conductivity of the system, so the Fe-GY shows a significant metallicity compared to Co-GY and Ni-GY.

The Mulliken population analysis shows that the lost net charges are 0.140*e* for Fe, 0.120*e* for Co, and 0.130*e* for Ni, respectively. The PDOS analysis further indicates that the electrons displaced from the TM atoms are predominantly relocated to C_{2p} orbitals. The CDD shows that the interaction of the doped TM atom with the γ-GY results in charge redistribution and electron accumulation around the TM–C bond (Fig. 5), indicating that chemical bonds may form between TM and its adjacent C atoms.[54–56] Furthermore, there is internal regional hybridization of the electrons of the metal atom itself. The electrical characteristics of biomolecules determine the sensing capabilities within the system under study, which can be demonstrated by their behavior before and after adsorption.

3.2 Analysis of the RB adsorption performance of the γ-GY

Fig. 6 displays the electrostatic potential isosurface (ESP) of the RBs, with blue indicating positive potential regions and red indicating negative potential regions. In RBs, negatively charged active groups have a significant effect on cellular metabolism. The RBs are placed approximately 3 Å away from the γ-GY nanosheets in a parallel (π–π) or vertical (σ–π) orientation for optimal configuration. The optimization results show that the optimal structure is π–π stacked, and the geometry and properties are displayed in Table 2 and Fig. S4 (ESI†), which aligns well with earlier published research.[57] The adsorption energy on γ-GY is −0.57 eV (Cyt), −0.79 eV (5-meCyt), −0.71 eV (5-hmCyt), −0.67 eV (5-caCyt) and −0.61 eV (5-fCyt), respectively. When interacting with γ-GY, the adsorption strength of RBs is as follows: 5-meCyt > 5-hmCyt > 5-caCyt > 5-fCyt > Cyt. It is worth noting that the adsorption energy and distance analysis shows that this adsorption is physisorption. In a word, the adsorption of RBs by γ-GY is a result of a synergistic effect, with the variation in the interactions associated with the distinct electronic states of the C atoms.

As a semiconductor material, it is significant to study the electronic behavior of the RBs with the substrate. The adsorption of RBs increases the energy levels located below the Fermi level, which is a consequence of the orbital hybridization between the RBs and γ-GY (Fig. S5, ESI†). As seen from Table 2, the band gaps of the RBs with γ-GY are 0.439 eV (Cyt), 0.451 eV (5-meCyt), 0.454 eV (5-hmCyt), 0.440 eV (5-caCyt) and 0.438 eV (5-fCyt), respectively. In Fig. S5 (ESI†), we observe that the PDOS in the γ-GY system at the orbital level shows no abrupt change in Fermi energy, only a slight change in the bond

Published on 24 September 2024. Downloaded on 4/12/2026 3:20:09 PM.

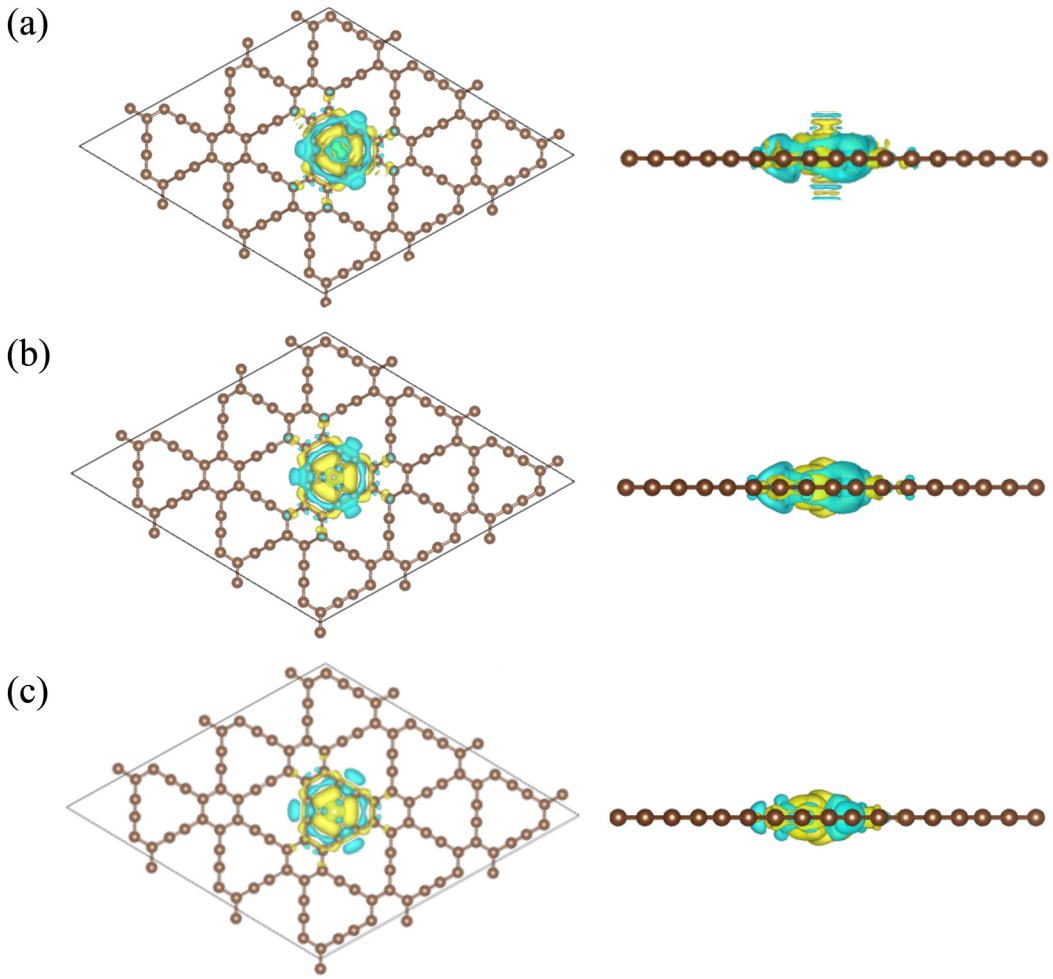

Fig. 5 The CDD of (a) Fe-GY, (b) Co-GY, and (c) Ni-GY (top and side view). The yellow and blue are the charge accumulation and depletion, respectively.

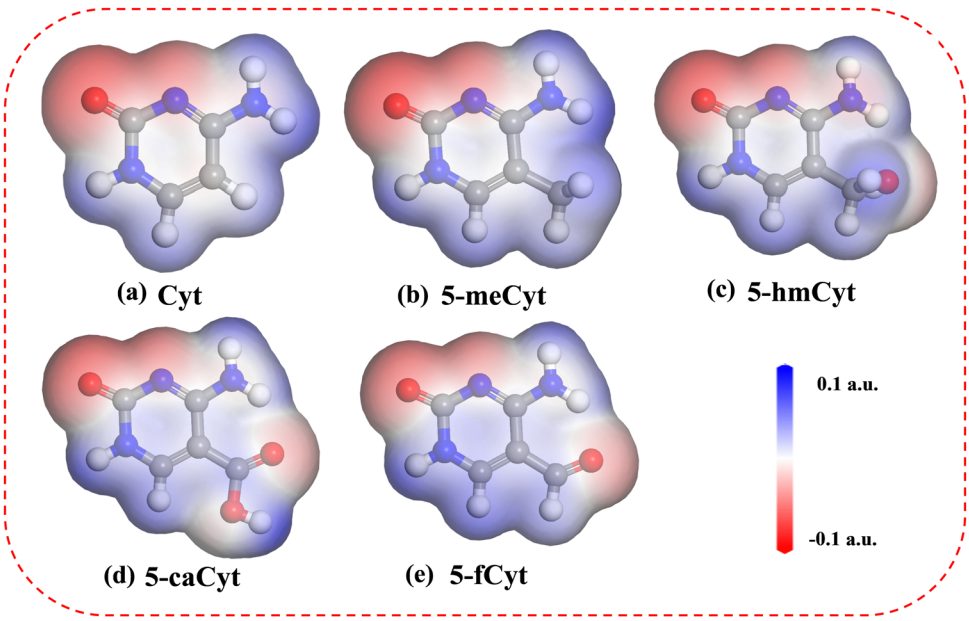

Fig. 6 ESP of (a) Cyt, (b) 5-meCyt, (c) 5-hmCyt, (d) 5-caCyt and (e) 5-fCyt (0.05 a.u.).

 This journal is © the Owner Societies 2024

Published on 24 September 2024. Downloaded on 4/12/2026 3:20:09 PM.

Table 2 Adsorption energy (E_{ads}/eV), distances (d/Å), charge transfer (Q/e), energy gap (E_g/eV), gap variation (ΔE_g/%), translocation time (τ/s), and sensing response (S%)

System	E_{ads}	d	Q	E_g	ΔE_g	τ	S (%)
γ-GY				0.452			
Cyt	−0.57	3.149	0.028	0.439	2.9	3.9×10^{-6}	28.8
5-meCyt	−0.79	3.129	0.029	0.451	0.3	2.5×10^{-2}	1.97
5-hmCyt	−0.71	3.077	0.019	0.454	0.4	8.9×10^{-4}	3.81
5-caCyt	−0.67	3.163	0.008	0.440	2.7	2.6×10^{-4}	26.31
5-fCyt	−0.61	3.152	0.009	0.438	3.1	2.4×10^{-5}	31.3
Fe-GY				0.238			
Cyt	−1.45	2.006	0.206	0.150	37.0	2.63×10^{9}	448.56
5-meCyt	−1.14	2.882	0.086	0.380	59.7	1.70×10^{4}	93.59
5-hmCyt	−1.28	2.008	0.304	0.304	27.7	3.67×10^{6}	72.10
5-caCyt	−1.19	2.000	0.253	0.346	45.4	1.20×10^{5}	87.62
5-fCyt	−1.20	1.996	0.244	0.357	50.0	1.36×10^{5}	89.99
Co-GY				0.352			
Cyt	−1.24	2.220	0.254	0.418	18.8	6.00×10^{6}	72.10
5-meCyt	−1.29	2.218	0.262	0.414	17.6	4.54×10^{6}	69.86
5-hmCyt	−1.26	2.225	0.258	0.362	2.9	1.27×10^{6}	17.59
5-caCyt	−1.13	2.246	0.229	0.389	10.5	8.99×10^{3}	51.11
5-fCyt	−1.28	2.209	0.218	0.458	30.1	3.29×10^{6}	87.13
Ni-GY				0.439			
Cyt	−0.92	3.326	0.038	0.430	2.0	2.91×10^{0}	19.01
5-meCyt	−1.06	3.249	0.052	0.430	2.0	6.81×10^{2}	19.01
5-hmCyt	−1.14	3.262	0.045	0.431	1.82	1.27×10^{4}	16.73
5-caCyt	−1.02	3.263	0.002	0.437	0.46	1.23×10^{2}	3.94
5-fCyt	−0.96	3.272	0.014	0.438	0.23	1.60×10^{1}	1.95

state. Additionally, according to the Mulliken charge analysis, the RBs transferred 0.008–0.029e to γ-GY, making the RBs electron donors. The fewer electrons transferred between RBs and γ-GY exhibit a notably weak physical interaction, which is consistent with the band gap and PDOS diagram.

From a theoretical point of view, the translocation time and sensing response are equally pivotal in dictating the performance of sensor materials beyond the commonly considered parameters such as adsorption energy, band structure, and electron charge transfer. As seen from Table 2, it is observed that the translocation time increases exponentially in relation to the adsorption energy. The γ-GY nanosheets exhibit varying translocation times for different RBs: 3.9×10^{-6} s for Cyt, 2.5×10^{-2} s for 5-meCyt, 8.9×10^{-4} s for 5-hmCyt, 2.6×10^{-4} s for 5-caCyt and 2.4×10^{-5} s for 5-fCyt, respectively. Among these bases, 5-meCyt is associated with the longest translocation time, while Cyt has the shortest. Besides, the translocation times for 5-hmCyt and 5-fCyt are notably similar, which complicates their differentiation.

The sensing response, which is dependent on the alteration of conductivity, is a critical measure for assessing the efficacy of electrical sensors. The γ-GY nanosheets have a sensing response of 28.8% for Cyt, 1.97% for 5-meCyt, 3.81% for 5-hmCyt, 26.31% for 5-caCyt and 31.3% for 5-fCyt, respectively. The results indicate that the sensing response values are notably low, which complicates the clear differentiation of RBs. This challenge is particularly pronounced in the case of distinguishing between 5-meCyt and 5-hmCyt.

3.3 Analysis of the RB adsorption performance of TM-GY

Pristine γ-GY exhibits inadequate sensitivity towards RBs, which is a critical limitation for its application in biomolecular

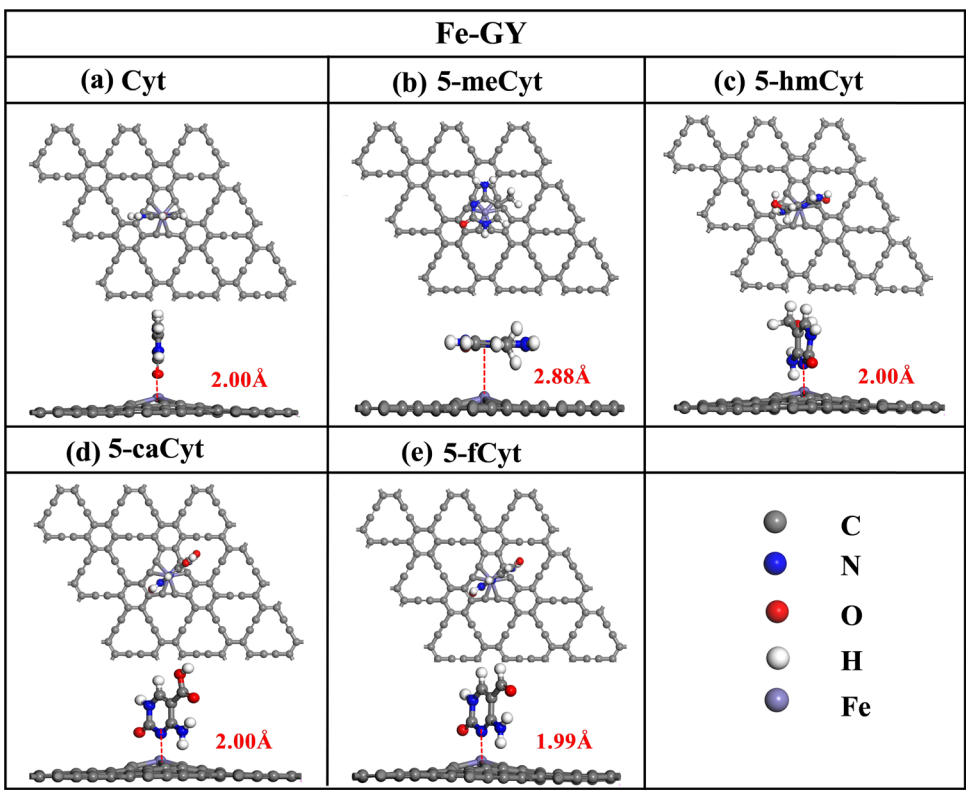

Fig. 7 Optimized geometries of (a) Cyt, (b) 5-meCyt, (c) 5-hmCyt, (d) 5-caCyt, and (e) 5-fCyt absorbed on the Fe-GY system (top and side perspective).

Published on 24 September 2024. Downloaded on 4/12/2026 3:20:09 PM.

detection. Upon doping, the structural and electronic characteristics of γ-GY undergo significant alterations, which are of considerable importance for the detection of biomolecules. Several different adsorption orientations are considered to determine the most suitable adsorption model for RBs with TM-GY (Table S1, ESI†). The lowest energy and most favorable conformation are shown in Fig. 7 and Fig. S6, S7 (ESI†). It is worth noting that when RBs are adsorbed on Fe-GY with rich adsorption orientations, and when RBs are adsorbed on Co-GY and Ni-GY with a single adsorption orientation, no significant deformation is observed in all TM-GY substrates.

The calculations show that the adsorption energies of the Fe-GY and Co-GY are greater than those of Ni-GY systems. The adsorption energy on Fe-GY is −1.45 eV (Cyt, –CO end), −1.14 eV (5-meCyt, –PP end), −1.28 eV (5-hmCyt, ═N end), −1.19 eV (5-caCyt, ═N end) and −1.20 eV (5-fCyt, ═N end) at adsorption distances of 2.006, 2.882, 2.008, 2.000 and 1.996 Å, respectively. The RBs have strong adsorption in the Fe-GY system, and the order is as follows: Cyt > 5-hmCyt > 5-fCyt > 5-caCyt > 5-meCyt. Other RBs are adsorbed on the Co-GY in a σ–π orientation, and the adsorption energy is between −1.13 eV and −1.28 eV, with an adsorption distance of about 2.2 Å. The order is as follows: 5-meCyt > 5-fCyt > 5-hmCyt > Cyt > 5-caCyt. We notice a tendency that the shorter the adsorption distances, the stronger the associated interaction. Similarly, the RBs are adsorbed on the Ni-GY system in a π–π orientation and the maximum adsorption distance of Cyt is 3.272 Å. The order is as follows: 5-hmCyt > 5-meCyt > 5-caCyt > 5-fCyt > Cyt. The results show that the interaction of RBs in the TM-GY system is significantly greater than that in the γ-GY system.

The electronic properties and adsorption behavior of materials can be elucidated more effectively by employing band structure and PDOS plot analysis (Fig. 8 and Fig. S8–S10, ESI†). The adsorption of the RBs significantly alters the electronic structure of TM-GY. Interestingly, the band gap of the adsorption system is changed to different degrees compared with γ-GY. The band gap of Fe-GY is decreased with the adsorption of Cyt, and the Cyt-Fe-GY system has the largest degree of upward movement of the valence band, resulting in a minimum band gap. With the adsorption of 5-meCyt, 5-hmCyt, 5-caCyt, and 5-fCyt, the band gap of the Fe-GY system increased, but the bandgap as a whole decreased compared to the γ-GY adsorption system, which is the result of the coupling of RBs with different orbital electrons of TM-GY. For the Co-GY system, the adsorption of RBs leads to the increase of the band gap of the system to varying degrees. Besides, for the Ni-GY system, the adsorption of RBs slightly reduces the band gap of the system.

In all adsorption systems, the overall DOS is predominantly from the C_{2p} orbital. The adsorption of RBs results in a heightened intensity of the peak at the Fermi level and the elevation of the energy of the system, and there is a clear overlap between the p and d orbitals between the adsorbed systems. In Fig. 9,

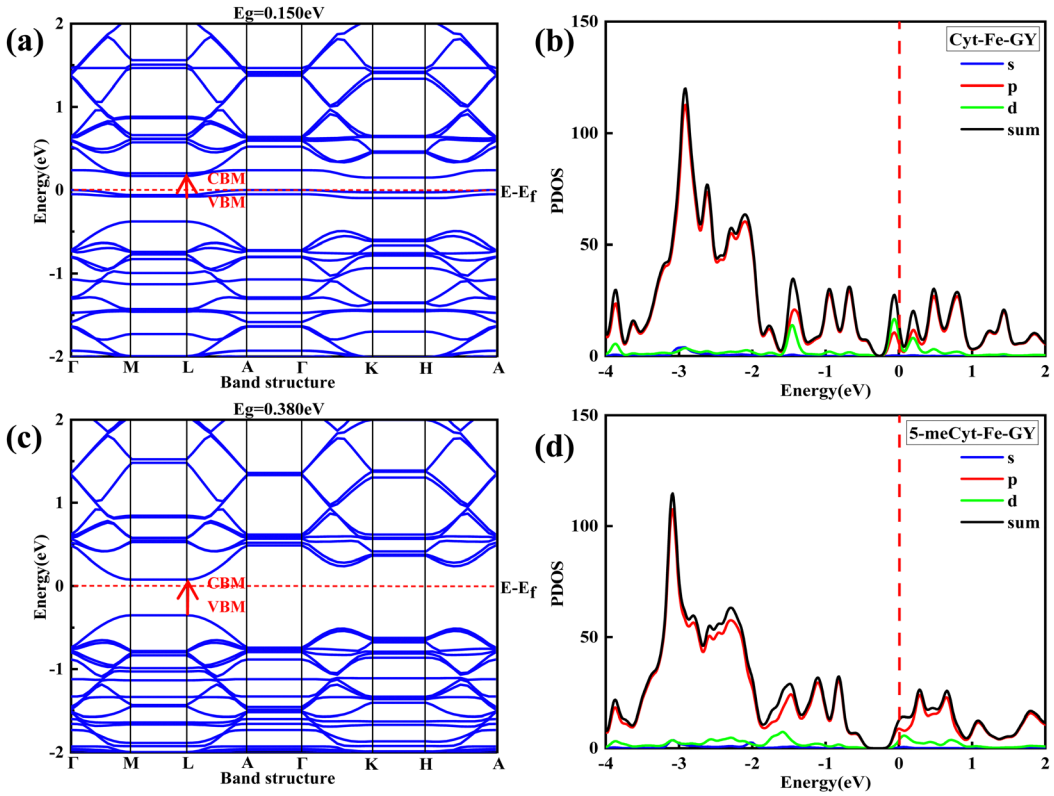

Fig. 8 Band structure (left) of (a) Cyt and (c) 5-meCyt absorbed on Fe-GY nanosheets, and DOS plot (right) of (b) Cyt and (d) 5-meCyt absorbed on Fe-GY nanosheets. The Fermi level is set to zero.

 This journal is © the Owner Societies 2024

Published on 24 September 2024. Downloaded on 4/12/2026 3:20:09 PM.

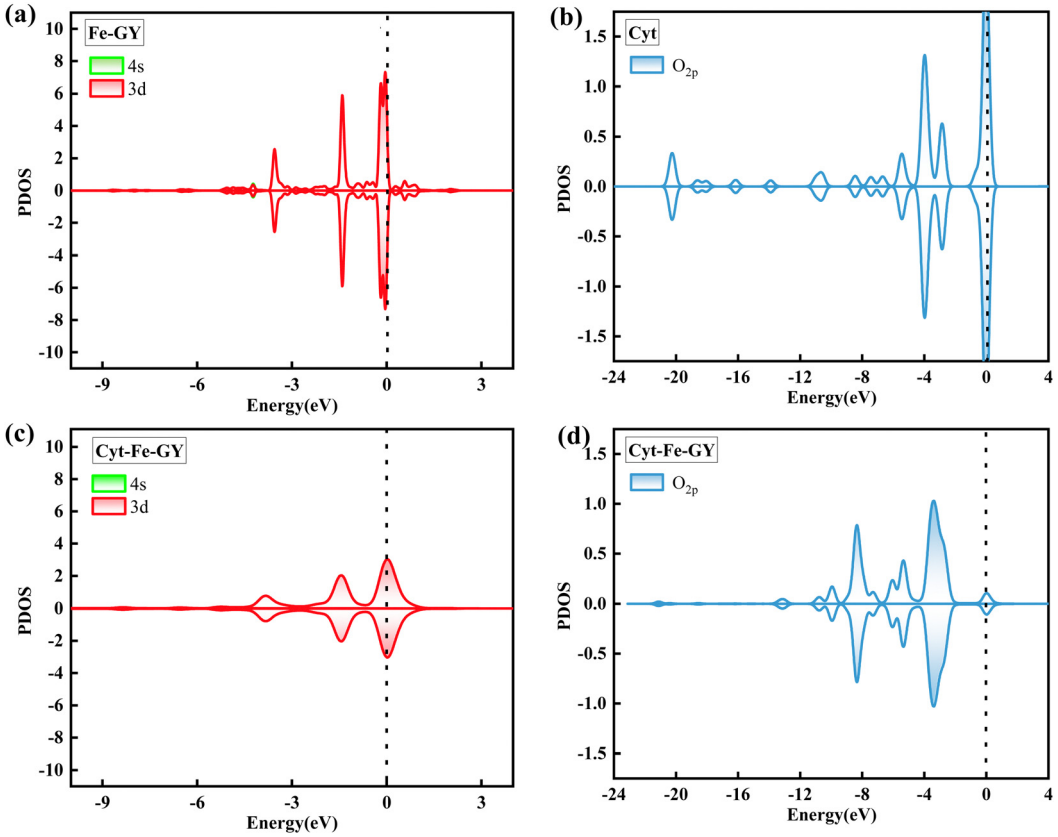

Fig. 9 PDOS plots: a comparison of the Fe valence orbitals between (a) Fe-GY and (c) Cyt-Fe-GY in the left panel; the comparison of the O_{2p} of (b) the standalone Cyt with those within (d) the Cyt-Fe-GY system in the right panel.

the left figure of the PDOS compares the valence orbitals of Fe atoms in the Fe-GY and Cyt-Fe-GY systems. The right figure compares the O_{2p} orbitals of the Cyt and Cyt-Fe-GY systems. When Cyt interacts with the Fe-GY system, the energy level of the O_{2p} orbital in Cyt drops below the Fermi level, indicating that charge transfer has occurred from the O_{2p} orbital in Cyt. In Cyt-Fe-GY, the 3d orbital of Fe shows some degree of broadening at the peak near the Fermi level, indicating that electrons are accumulating. The orbital interactions exhibit similarities between other RBs and Fe-GY systems, as seen in Fig. S11 (ESI†). For the Cyt-Co-GY system (Fig. S12, ESI†), the energy state of the N_{2p} orbital in Cyt decreases at the Fermi level, and the 3d 4s orbitals of Co in the Cyt-Co-GY system have new peaks at the Fermi level, which emphasizes the direction of electron transfer. The orbital interactions exhibit similarities between other RBs and Co-GY systems. In contrast, when RBs are adsorbed in the Ni-GY system, they exert a negligible influence on the electronic state of the Ni-GY, so there is no comparison of the density of states here. The significant adsorption of RBs on the Fe/Co-GY is predominantly attributed to the charge transfer of the valence orbitals of O/N atoms and TM atoms, and the hybridization occurs at different orbital electron energy levels.

The Mulliken charge analysis provides information on charge transfer, and all the RBs experience charge loss (Table 2). In the Fe-GY system, 5-meCyt has a minimum charge loss of 0.086*e*, and 5-hmCyt has a maximum charge loss of 0.304*e*. At the same time, the overall charge loss of the Co-GY system from the RBs is stable at 0.254*e* (Cyt), 0.262*e* (5-meCyt), 0.258*e* (5-hmCyt), 0.229*e* (5-caCyt) and 0.218*e* (5-fCyt), respectively. Note that RBs have minimal electron transfer in the Ni-GY system, ranging from 0.003–0.050*e*, which was almost negligible. With the transfer of charge, the transfer of charge predominantly exists in the vicinity of the transition metal-doped 12C ring and RBs molecules in the Fe-GY and Co-GY systems (Fig. 10 and Fig. S13, S14, ESI†), indicating that the introduction of Fe and Co atoms destroys the inertness of the surface and increases the sensitivity to RB molecules. The charge transfer and redistribution are in line with the PDOS findings and reflect the electron-donating properties of the RB molecules. The RB molecules show high adsorption energy, electron orbital displacement, and charge transfer on Fe-GY and Co-GY systems, and have obvious chemisorption. The magnitude of the charge transfer between RBs and TM-GY directly influences the extent of the band gap change. Additionally, the sensitivity of TM-GY is directly proportional to the magnitude of the charge transfer in TM-GY.

Among all the adsorption systems, Cyt-Fe-GY has the longest translocation time of 2.63×10^9 s, which is consistent with its strong chemical adsorption. In general, a high adsorption energy is associated with prolonged translocation times, which hinders the efficient utilization of the sensor in practical

Published on 24 September 2024. Downloaded on 4/12/2026 3:20:09 PM.

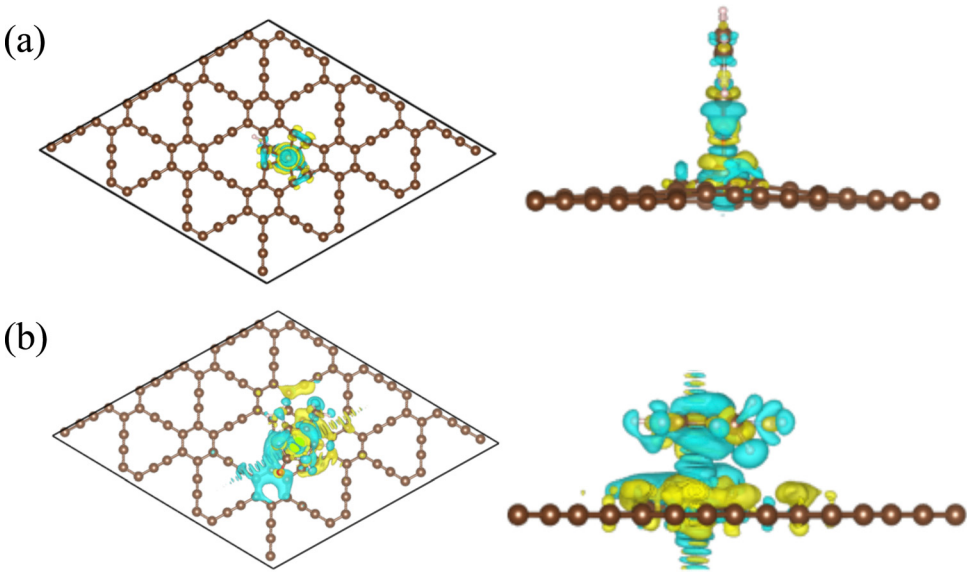

Fig. 10 The CDD of (a) Cyt-Fe-GY and (b) 5-meCyt-Fe-GY (top and side view). The yellow and blue are the charge accumulation and depletion, respectively.

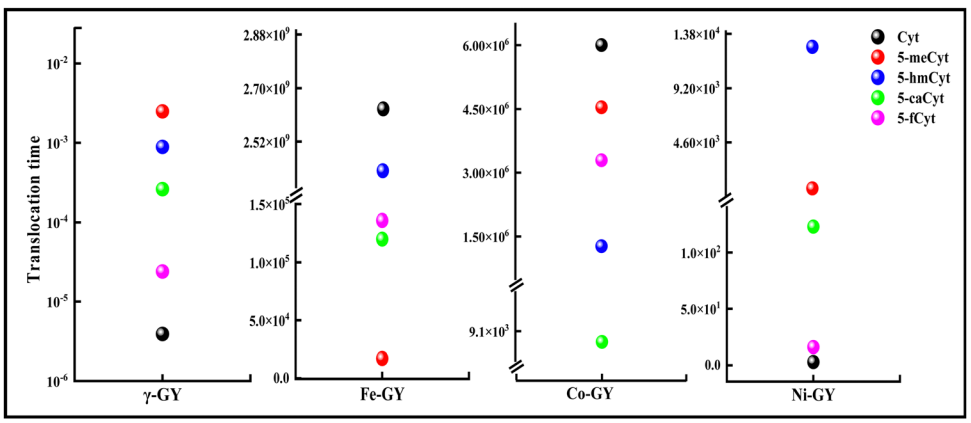

Fig. 11 Translocation time of RBs adsorbed on γ-GY and TM-GY nanosheets.

applications. This issue can be addressed by optimizing the operating frequency and adjusting the temperature.[58] For the Co-GY system, except for 5-caCyt, which has a short translocation time (about 10^3 s), the translocation time of the remaining bases is in the range of 10^6 s. Compared with Fe-GY and Co-GY systems, the RBs adsorbed on Ni-GY have the best translocation performance with shorter translocation time, which is 2.91×10^0 s for Cyt, 6.81×10^2 s for 5-meCyt, 1.27×10^4 s for 5-hmCyt, 1.23×10^2 s for 5-caCyt and 1.60×10^1 s for 5-fCyt, respectively. From these, the gradient of the translocation time changes is sufficient to distinguish each rare base molecule (Fig. 11).

According to eqn (5), the sensing response is fundamentally determined by the magnitude of $|\Delta E_g|$, representing the difference in the E_g between the TM-GY and the RBs with the TM-GY system. Specifically, the Fe-GY system has the greatest variation in E_g, with a maximum ΔE_g of 59%, which results in a very high sensitivity response, indicating the potential of Fe-GY as an RB detection device. For the Co-GY system, 5-caCyt has the highest sensitivity, and 5-meCyt has the lowest response according to the change in value of the band gap. The sensing response of the RBs with Co-GY nanosheets follows the order: 5-fCyt > Cyt > 5-meCyt > 5-caCyt > 5-hmCyt, which is consistent with our speculation. In contrast, the band gap of the Ni-GY system has no obvious changes, which may result in a low sensing response. In short, Fe-GY has the best sensitive response, followed by Co-GY and finally Ni-GY system (Fig. 12).

3.4 Sensing response analysis of RBs on Ni-GY with an electric field

Previous studies have shown that applying an electric field can effectively regulate the band gap.[59,60] For RBs on Ni-GY adsorption systems, it is difficult to distinguish each base directly from the sensitive response value, so the band gap can be effectively regulated by applying a vertical electric field. Fig. S15 (ESI†)

 This journal is © the Owner Societies 2024

Published on 24 September 2024. Downloaded on 4/12/2026 3:20:09 PM.

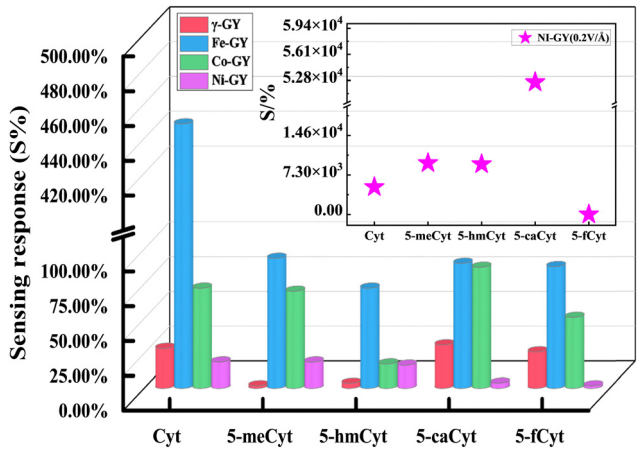

Fig. 12 Sensing response of RBs adsorbed on γ-GY and TM-GY nanosheets, the inset shows the sensing response of RBs adsorbed on Ni-GY nanosheets in a 0.2 V Å^{-1} electric field.

presents the band diagrams for the Ni-GY system upon adsorption of RBs in a 0.2 V Å^{-1} electric field. The calculation analysis reveals the band gap of the adsorbed system changes greatly under the specified electric field conditions. The reason is that the potential difference introduced by the external electric field changes the energy level and energy difference between the VBM and CBM, thus changing the gap. The Ni-GY has band gaps of RBs: 0.215 eV (Cyt), 0.183 eV (5-meCyt), 0.184 eV (5-hmCyt), 0.095 eV (5-caCyt) and 0.431 eV (5-fCyt), respectively. According to eqn (5), the Ni-GY nanosheets have a sensing response of 5071.98% for Cyt, 9504.31% for 5-meCyt, 9320.32% for 5-hmCyt, 52585.46% for 5-caCyt and 20.71% for 5-fCyt, respectively. In this way, RBs can be easily identified in only a 0.2 V Å^{-1} electric field.

In general, the TM-GY nanosheets are expected to be used as sensing materials for distinguishing RBs in DNA based on distinct characteristic properties different from the γ-GY.

4. Conclusion

The adsorption behavior of RBs on γ-GY and TM-GY nanosheets has been studied based on the first-principles calculations of density functional theory. The augments in the specific area of γ-GY after doping can provide more active sites and the electron flow of electron increases along with charge transfer and charge redistribution. The interaction of γ-GY with RBs can be described as weak and physisorption, which makes it difficult to clearly distinguish between each base molecule. Apparently, the adsorption capacity of the system doped with Fe, Co, and Ni was significantly improved. In the analysis of translocation time, the Fe-, Co-, and Ni-GY systems exhibit exceptional efficiency in distinguishing RBs, with Ni-GY demonstrating superior performance compared to the others. Regarding sensing response, Fe-GY systems have shown strong capability in detecting RBs, with response intensities as follows: Fe-GY: Cyt (448.56%) > 5-meCyt (93.59%) > 5-fCyt (89.99%) > 5-caCyt (87.62%) > 5-hmCyt (72.10%). Furthermore, the Ni-GY can be used for detection purposes in terms of sensing response under the action of an applied electric field. The proposed method can detect targeted nucleobases with good translocation time and sensitivity, enabling advances in personalized medicine and universal cancer screening tests.

Data availability

The data that support the findings of this study are available from the corresponding author upon reasonable request.

Conflicts of interest

There are no conflicts to declare.

Acknowledgements

The authors acknowledge the financial support from the National Natural Science Foundation of China (22177066, 12174238, 92261023), the Natural Science Foundation of Shaanxi Province (2023-YBGY-486, 23JHQ073), the Department of Education Project (23JP023), the Co-construction Project of Hanzhong city and Shaanxi University of Technology (SXJ-2107, SXC-2104), and the Innovation Team of Shaanxi Universities (2022-94).

References

1 Q. Li, H. Liu, Y. Tian, J. Guo, G. Chen and J. Y. Lee, *J. Phys. Chem. C*, 2020, **4**, 10823–10831, DOI: **10.1021/acs.jpcc.0c01734**.
2 G. D. Riso, D. F. G. Fiorillo, A. Fierro, M. Cuomo, L. Chiariotti, G. Miele and S. Cocozza, *Biomolecules*, 2020, **10**, 1271–1285, DOI: **10.3390/biom10091271**.
3 V. B. Teif and A. G. Cherstvy, *AIMS Biophys.*, 2020, **3**, 88–98, DOI: **10.3934/biophy.2016.1.88**.
4 A. G. Cherstvyand and R. G. WinklerJ, *Phys. Chem. B*, 2005, **109**, 2962–2969, DOI: **10.1021/jp0462299**.
5 K. D. Rasmussen and K. Helin, *Genes Dev.*, 2016, **30**, 733–750, DOI: **10.1101/gad.276568.115**.
6 F. R. Traube and T. Carell, *RNA Biol.*, 2017, **14**, 1099–1107, DOI: **10.1080/15476286.2017.1318241**.
7 P. A. Jones and D. Takai, *Science*, 2001, **293**, 1068–1070, DOI: **10.1126/science.1063852**.
8 H. Gowher and A. Jeltsch, *Biochem. Soc. Trans.*, 2018, **46**, 1191–1202, DOI: **10.1042/bst20170574**.
9 M. Münzel, D. Globisch and T. Carell, *Angew. Chem., Int. Ed.*, 2011, **50**, 6460–6468, DOI: **10.1002/anie.201101547**.
10 E. Povedano, V. R. V. Montiel, A. Valverde and F. Navarro-Villoslada, *ACS Sens.*, 2019, **4**, 227–234, DOI: **10.1021/acssensors.8b01339**.
11 L. Krejcova, L. Richtera, D. Hynek, J. Labuda and V. Adam, *Biosens. Bioelectron.*, 2017, **97**, 384–399, DOI: **10.1016/j.bios.2017.06.004**.

Published on 24 September 2024. Downloaded on 4/12/2026 3:20:09 PM.

12 K. S. Novoselov, A. K. Geim, S. V. Morozov, D. Jiang, Y. Zhang and S. V. Dubonos, *Science*, 2004, **22**, 666–669, DOI: **10.1126/science.1102896**.
13 S. K. Jana, D. Chodvadiya, N. N. Som and P. K. Jha, *Diamond Relat. Mater.*, 2022, **129**, 109305, DOI: **10.1016/j.diamond.2022.109305**.
14 D. Wu, S. Wang, S. Zhang, Y. Liu, Y. Ding, B. Yang and H. Chen, *Phys. Chem. Chem. Phys.*, 2019, **21**, 1029–1037, DOI: **10.1039/c8cp05008b**.
15 H. Li, W. Fu, K. Xu, C. Wang, Y. Li, J. Zhang, W. Jiang, W. Zhu and H. Li, *J. Mol. Graphics Modell.*, 2020, **94**, 107475, DOI: **10.1016/j.jmgm.2019.107475**.
16 Y. Li, H. Wang, L. Xie, Y. Liang, G. Hong and H. Dai, *J. Am. Chem. Soc.*, 2011, **133**, 7296–7299, DOI: **10.1021/ja201269b**.
17 D. Cortés-Arriagada, *J. Mol. Liq.*, 2021, **329**, 115229, DOI: **10.1016/j.molliq.2020.115229**.
18 E. T. Alonso, D. P. Rodrigues, M. Khetani and D. W. Shin, *npj Flexible Electron.*, 2018, **2**, 25–31, DOI: **10.1038/s41528-018-0040-2**.
19 X. Li, J. Yu, S. Wageh, A. A. Al-Ghamdi and J. Xie, *Small*, 2016, **12**, 6640–6696, DOI: **10.1002/smll.201600382**.
20 N. Duhan and T. J. Dhilip Kumar, *Appl. Surf. Sci.*, 2024, **642**, 158553, DOI: **10.1016/j.apsusc.2023.158553-158562**.
21 N. Barman, J. Deb and U. Sarkar, *Appl. Surf. Sci.*, 2023, **640**, 158473, DOI: **10.1016/j.apsusc.2023.158473-158470**.
22 R. Liu, J. Zhou, X. Gao, J. Li, Z. Xie, Z. Li, S. Zhang, L. Tong, J. Zhang and Z. Liu, *Adv. Electron. Mater.*, 2017, **3**, 1700122, DOI: **10.1002/aelm.201700122**.
23 H. Qiu, M. Xue, C. Shen, Z. Zhang and W. Guo, *Adv. Mater.*, 2019, **31**, e1803772, DOI: **10.1002/adma.201803772**.
24 W. T. Yang, B. Zhao, C. Y. Li, P. Guo, M. Li, X. H. Ge, M. Zhang, X. Y. Guan and J. J. Wang, *Appl. Surf. Sci.*, 2023, **640**, 158473, DOI: **10.1016/j.apsusc.2022.154083**.
25 L. Wu, J. Gao, X. Lu, C. Huang, Dhanjai and J. Chen, *Carbon*, 2020, **156**, 568–575, DOI: **10.1016/j.carbon.2019.09.086**.
26 R. H. Baughman, H. Eckhardt and M. Kertesz, *J. Chem. Phys.*, 1987, **87**, 6687–6699, DOI: **10.1063/1.453405**.
27 G. Li, Y. Li, H. Liu, Y. Guo, Y. Li and D. Zhu, *Chem. Commun.*, 2010, **46**, 3256–3258, DOI: **10.1039/b922733d**.
28 J. Liu, C. Chen and Y. Zhao, *Adv. Mater.*, 2019, **31**, e804386, DOI: **10.1002/adma.201804386**.
29 Q. Li, Y. Li, Y. Chen, L. Wu, C. Yang and X. Cui, *Carbon*, 2018, **136**, 248–254, DOI: **10.1016/j.carbon.2018.04.081**.
30 S. Lakshmy, A. Kundu, N. Kalarikkal and B. Chakraborty, *J. Mater. Chem. B*, 2022, **10**, 5958–5967, DOI: **10.1039/d2tb00754a**.
31 M. Cui, Z. Che, Y. Gong, T. Li, W. Hu and S. Wang, *Chem. Eng. J. Adv.*, 2022, **431**, 133455, DOI: **10.1016/j.cej.2021.133455**.
32 S. Madhumitha, V. Nagarajan and R. Chandiramouli, *Comput. Theor. Chem.*, 2019, **1163**, 112514, DOI: **10.1016/j.comptc.2019.112514**.
33 R. L. Kumawat and B. Pathak, *ACS Appl. Electron. Mater.*, 2021, **3**, 3835–3845, DOI: **10.1021/acsaelm.1c00452**.
34 S. Chandra Shekar and R. S. Swathi, *J. Phys. Chem. C*, 2014, **118**, 4516–4528, DOI: **10.1021/jp412791v**.
35 M. Lv, R. Li, X. Zeng, L. Jin, C. Zhao, Y. Gao, M. Jiang, G. Qin, C. Li and S. Zhang, *Phys. Chem. Chem. Phys.*, 2023, **25**, 10472–10480, DOI: **10.1039/d2cp04648b**.
36 R. R. Li, X. Zeng, M. D. Lv, R. Y. Zhang, S. R. Zhang, T. L. Zhang, X. H. Yu, C. Li, L. X. Jin and C. B. Zhao, *Phys. Chem. Chem. Phys.*, 2024, **26**, 5558–5568, DOI: **10.1039/d3cp04726a**.
37 B. Delley, *J. Chem. Phys.*, 2000, **113**, 7756–7764, DOI: **10.1063/1.1316015**.
38 J. P. Perdew, K. Burke and M. Ernzerhof, *Phys. Rev. Lett.*, 2002, **77**, 3865–3868, DOI: **10.1103/physrevlett.77.3865**.
39 J. P. Perdew, J. A. Chevary, S. H. Vosko, K. A. Jackson, M. R. D. J. Pederson and C. S. Fiolhais, *Phys. Rev. B: Condens. Matter Mater. Phys.*, 2002, **48**, 4978, DOI: **10.1103/physrevb.48.4978.2**.
40 S. Grimme, *J. Comput. Chem.*, 2006, **27**, 1787–1799, DOI: **10.1002/jcc.20495**.
41 M. D. Ganji, H. Ko, S. Jamehbozorgi, M. Tajbakhsh, S. Tanreh, R. P. Nejad, M. Sepahvandf and M. Rezvani, *Phys. Chem. Chem. Phys.*, 2024, **26**, 14018–14036, DOI: **10.1039/d3cp01490h**.
42 B. Delley, *J. Chem. Phys.*, 1990, **92**, 508–517, DOI: **10.1063/1.458452**.
43 H. J. Monkhorst and J. D. Pack, *Phys. Rev. B: Condens. Matter Mater. Phys.*, 2002, **39**, 3168–3172, DOI: **10.1103/physrevb.13.5188**.
44 T. Hu and J. Hong, *J. Phys. Chem. C*, 2015, **119**, 8199–8207, DOI: **10.1021/acs.jpcc.5b01300**.
45 S. Kim, A. R. Puigdollers, P. Gamallo, F. Viñes and J. Y. Lee, *Carbon*, 2017, **120**, 63–70, DOI: **10.1016/j.carbon.2017.05.028**.
46 U. Srimathi, V. Nagarajan and R. Chandiramouli, *J. Mol. Liq.*, 2018, **265**, 199–207, DOI: **10.1016/j.molliq.2018.05.114**.
47 A. Ghosh, B. Ball, S. Pal and P. Sarkar, *J. Phys. Chem. Lett.*, 2022, **13**, 7898–7905, DOI: **10.1021/acs.jpclett.2c02196**.
48 L. Shabtay and A. M. Boris, *Phys. Optics*, 2018, **1101**, 5772, DOI: **10.1103/physreva.83.023807**.
49 H. H. Gürel and B. Salmankurt, *Biosensors*, 2021, **11**, 11–59, DOI: **10.3390/bios11030059**.
50 S. Kim, P. Gamallo, F. Viñes and J. Y. Lee, *Appl. Surf. Sci.*, 2020, **114**, 143927, DOI: **10.1016/j.apsusc.2019.143927**.
51 Y. F. Zhang, T. Gao, T. Y. Zhang and Z. F. Liu, *Acta Phys. Chim. Sin.*, 2012, **28**, 2456–2464, DOI: **10.3866/PKU.WHXB201209062**.
52 S. J. Qin, Y. L. Liu, R. Li, Y. N. Jiao, H. B. Chen and J. J. Zhao, *J. Mater. Chem. A*, 2024, **12**, 5805–5814, DOI: **10.1039/d3ta07925b**.
53 D. K. Thomas, I. Marcella and D. B. Mauro, *J. Chem. Phys.*, 2020, **152**, 194103, DOI: **10.1063/5.0007045**.
54 T. Lu and F. W. Chen, *J. Comput. Chem.*, 2012, **33**, 580–592, DOI: **10.1002/jcc.22885**.
55 G. Kresse and J. Furthmüller, *Comput. Mater. Sci.*, 1996, **6**, 15–50, DOI: **10.1016/0927-0256(96)00008-0**.
56 V. Wang, N. Xu, J. C. Liu, G. Tang and W. T. Geng, *Comput. Phys. Commun.*, 2021, **267**, 108033, DOI: **10.1016/j.cpc.2021.108033**.

 This journal is © the Owner Societies 2024

57 B. Li and Z. G. Shao, *Appl. Surf. Sci.*, 2020, **512**, 145635, DOI: **10.1016/j.apsusc.2020.145635**.
58 M. Mohammadzaheri, S. Jamehbozorgi, M. D. Ganji, M. Rezvani and Z. Javanshire, *Phys. Chem. Chem. Phys.*, 2023, **25**, 21492, DOI: **10.1039/d3cp05457h**.
59 K. X. Zhang, Y. F. Wang and Q. Xie, *J. Adv. Phys. Chem.*, 2024, **13**, 1–7, DOI: **10.12677/japc.2024.131001**.
60 Yj Lu, Y. Chen, F. C. Ye, L. B. Cai, Z. J. Dai and Y. P. Ren, *Acta Phys. Sin.*, 2024, **73**, 083101, DOI: **10.7498/aps.73.20231935**.

Published on 24 September 2024. Downloaded on 4/12/2026 3:20:09 PM.